Strong-field approximation for ionization of a diatomic molecule by a strong laser field. II. The role of electron rescattering off the molecular centers

M. Busuladžić,[1] A. Gazibegović-Busuladžić,[2] D. B. Milošević,[2,3] and W. Becker[3]
[1]*Medical Faculty, University of Sarajevo, Čekaluša 90, 71000 Sarajevo, Bosnia and Herzegovina*
[2]*Faculty of Science, University of Sarajevo, Zmaja od Bosne 35, 71000 Sarajevo, Bosnia and Herzegovina*
[3]*Max-Born-Institut, Max-Born-Strasse 2a, 12489 Berlin, Germany*
(Received 11 July 2008; published 11 September 2008)

The strong-field approximation for ionization of diatomic molecules by a strong laser field [D. B. Milošević, Phys. Rev. A **74**, 063404 (2006)] is generalized to include rescattering of the ionized electron wave packet off the molecular centers (the electron's parent ion or the second atom). There are four rescattering contributions to the ionization rate, which are responsible for the high-energy plateau in the electron spectra and which interfere in a complicated manner. The spectra are even more complicated due to the different symmetry properties of the atomic orbitals of which a particular molecular orbital consists. Nevertheless, a comparatively simple condition emerges for the destructive interference of all these contributions, which yields a curve in the $(E_{\mathbf{p}_f}, \theta)$ plane. Here θ is the electron emission angle and $E_{\mathbf{p}_f}$ is the electron kinetic energy. The resulting suppression of the rescattering plateau can be strong and affect a large area of the $(E_{\mathbf{p}_f}, \theta)$ plane, depending on the orientation of the molecule. We illustrate this using the examples of the $3\sigma_g$ molecular orbital of N_2 and the $1\pi_g$ molecular orbital of O_2 for various orientations of these molecules with respect to the laser polarization axis. For N_2, for perpendicular orientation and the equilibrium internuclear distance R_0, we find that the minima of the ionization rate form the curve $E_{\mathbf{p}_f} \cos^2 \theta = \pi^2/(2R_0^2)$ in the $(E_{\mathbf{p}_f}, \theta)$ plane. For O_2 the rescattering plateau is absent for perpendicular orientation.

DOI: 10.1103/PhysRevA.78.033412 PACS number(s): 33.80.Rv, 32.80.Rm, 42.50.Hz

I. INTRODUCTION

An atomic or molecular system irradiated by an intense laser field can be ionized by absorption of more photons than necessary for ionization: this process is called above-threshold ionization (ATI) (see, for example, the review article [1]). The motion of the center of the ionized electron wave packet follows approximately a classical trajectory. If the ionized electron goes directly to the detector we call this process "direct" ATI. The ionized electron may also return to its parent ion and recombine with it emitting a high-order harmonic: this is high-order harmonic generation. It is described by the three-step model, which includes ionization, propagation of the free electron in the laser field, and laser-assisted recombination, followed by harmonic emission [2]. On the other hand, the returning electron may also elastically scatter off its parent ion and then leave it towards the detector. In this case, the third step mentioned above is laser-assisted scattering. In this process, the electron can absorb many more photons from the laser field than in direct ATI. The high-energy ATI electrons were first observed in the experiments [3,4] and this process was named high-order ATI (HATI) or ATI with rescattering. The HATI electron energy spectrum forms a long plateau followed by a cutoff at $10U_p$ where U_p is the electron's ponderomotive energy (see, for example, the review articles [5–7]).

The laser-induced recombination and rescattering processes take place within a fraction of the laser-field cycle, which, for near-infrared pulses, is on the time scale of hundreds of attoseconds. This is the reason why these processes have recently attracted a lot of attention [7,8]. The laser-driven electrons rescatter off the parent ions. Since the molecules are multicenter systems, the rescattering electrons can serve to obtain the diffraction image of the parent molecule. For this it is important that, by new alignment techniques, it is possible to make sure that almost all molecules in the sample have the same orientation. Laser-induced electron diffraction for imaging molecules was proposed in Ref. [9]. Sub-laser-cycle rescattered electron pulses were suggested as a tool for probing the molecular dynamics [10]. The diffraction of these rescattering molecular photoelectrons was also analyzed in Refs. [11,12]. More recently, it was suggested that backscattered high-energy photoelectrons are most suitable to infer the electron-ion scattering potential [13]. Itatani *et al.* [14] have suggested a tomographic procedure for reconstructing the highest occupied molecular orbitals (HOMOs) using high-order harmonic generation. Since it is difficult to obtain accurate HOMO wave functions using this procedure, Le *et al.* [15] have suggested that using high-order harmonic generation some important information on the structure of a molecule can be extracted, such as geometry and symmetry of the HOMO, nodal surfaces, internuclear distances, etc. For a discussion of the emerging field of ultrafast molecular imaging using recolliding electron wave packets, see the recent review by Lein [16]. HATI can be considered as a pump-probe process with subfemtosecond time resolution. The ionization of the molecule by the laser field at a certain instant represents the pump process, while the recollision of the electron wave packet represents the probe process. In comparison with conventional electron diffraction the probability that an electron hits the target molecule is much larger in laser-induced recollision since the electron flux is much higher at the target position [10].

There are a few papers in which the rescattering high-energy electron energy spectra in molecular HATI were presented. Bandrauk *et al.* [17] have considered a one-

dimensional model of H_2^+ and H_3^{2+} by solving numerically the time-dependent Schrödinger equation. Similar calculations, but for a two-dimensional H_2^+ model were done by Lein *et al.* [18]. Plateaus much longer than the atomic $10U_p$ plateau, for very large internuclear distances, were predicted in Ref. [19] using a one-dimensional H_2^+ model. More recently, molecular HATI was considered using a two-center zero-range potential model [20]. The interference patterns in the electron spectra were analyzed and a method for determining the internuclear separation was proposed. In all the abovementioned papers the laser field was linearly polarized. It is interesting that for ionization of molecules by a circularly polarized few-cycle laser pulse plateau features (which are absent in the atomic ATI) appear due to the rescattering of electrons ionized at one center off the other center [21].

Molecules are multicenter systems. Therefore, ionization can take place at any one out of the two (or more) different centers, causing interference structures in the electron spectrum. In fact, even direct ionization without rescattering reveals the initial symmetry of the molecular system. For example, the O_2 molecule shows a suppression in the low-energy electron spectra due to its π symmetry, while the N_2 molecule, having σ symmetry, does not show such a suppression [22] (for a more recent experimental study see Ref. [23]). In Ref. [24] we have introduced a modified molecular strong-field approximation (MSFA) and have modeled the initial molecular state by the Slater-type orbitals obtained using the Hartree-Fock-Roothaan method. In the present paper we will improve this modified MSFA so that it includes the rescattering of the ionized electron off the atomic or ionic centers of which the molecule consists. The first results on this subject were presented in Ref. [25], where it was shown that the angle-resolved HATI molecular spectra can be used as a sensitive tool for molecular characterization. In the present paper we will elaborate on this and will give more examples. Our generalized MSFA theory is presented in Sec. II A. A physical picture of the ionization process, the interference of the partial T-matrix contributions, as well as the role of the molecular symmetry are considered in Sec. II B. In Sec. III we present and discuss our numerical results, first for the electrons emitted in the polarization direction (Sec. III A), and then we will analyze the angle and energy resolved molecular HATI spectra (Sec. III B). Finally, in Sec. IV we conclude with a summary.

II. THEORY

A. Generalized molecular strong-field approximation

We consider a diatomic molecule as a three-particle system, which consists of two heavy atomic (ionic) centers and an electron. In Ref. [24] it was shown that, after the separation of the center-of-mass coordinate, the dynamics of our system depend on the relative nuclear coordinate $\mathbf{R}=\mathbf{R}_B-\mathbf{R}_A$ and the electron coordinate $\mathbf{r}=\mathbf{r}_e-(M_A\mathbf{R}_A+M_B\mathbf{R}_B)/M_{AB}$ with respect to the nuclear center of mass. The masses (charges) of heavy particles are M_A and M_B (e_A and e_B), while the electron mass (charge) is m_e (e_e). The relative charges are defined by $e_r=[M_{AB}e_e-m_e(e_A+e_B)]/(M_{AB}+m_e)$ and $e_R=(M_Ae_B-M_Be_A)/M_{AB}$, with $M_{AB}=M_A+M_B$. The exact ionization probability amplitude is presented in [24] in the form

$$M_{fi}(t,t') = -i\int_{t'}^{t} d\tau \int d^3\mathbf{r}'d^3\mathbf{R}'\Phi_f^*(\mathbf{r}',\mathbf{R}',t) \times \int d^3\mathbf{r}d^3\mathbf{R}\langle \mathbf{r}',\mathbf{R}'|U(t,\tau)|\mathbf{r},\mathbf{R}\rangle \times V_F(\tau)\Phi_i(\mathbf{r},\mathbf{R},\tau), \quad (1)$$

where

$$V_F(\tau) = -(e_r\mathbf{r}+e_R\mathbf{R})\cdot\mathbf{E}(\tau) \quad (2)$$

is the interaction with the laser field in length gauge and dipole approximation. The function $\Phi_f(\mathbf{r},\mathbf{R},t)$ and the time evolution operator $U(t,\tau)$ correspond to the Hamiltonian

$$H(t) = \frac{\mathbf{P}^2}{2\mu}+\frac{\mathbf{p}^2}{2m}+V_F(t)+V(\mathbf{r},\mathbf{R}), \quad (3)$$

where the first two terms on the right-hand side are the kinetic energy operators, while the last term describes the interaction of the atomic (ionic) centers A and B with each other and with the electron in the absence of the laser field

$$V(\mathbf{r},\mathbf{R}) = V_e^{AB}(\mathbf{r},\mathbf{R})+V_{AB}(\mathbf{R}), \quad (4)$$

with

$$V_e^{AB}(\mathbf{r},\mathbf{R}) = V_e^A(\mathbf{r}_A)+V_e^B(\mathbf{r}_B), \quad (5)$$

and $\mathbf{r}_A=\mathbf{r}-(\lambda-1)\mathbf{R}/2$, $\mathbf{r}_B=\mathbf{r}-(\lambda+1)\mathbf{R}/2$, $\lambda=(M_A-M_B)/M_{AB}$ (we use the notation of Ref. [24]).

The MSFA was introduced in Ref. [24] by replacing Φ_f^*U in Eq. (1) with Φ_f^{F*}, where Φ_f^F is the solution of the time-dependent Schrödinger equation with the Hamiltonian H_F

$$H_F = h_e^F+H_{AB}^F, \quad h_e^F = \frac{\mathbf{p}^2}{2m}-e_r\mathbf{r}\cdot\mathbf{E}(t),$$

$$H_{AB}^F = \frac{\mathbf{P}^2}{2\mu}-e_R\mathbf{R}\cdot\mathbf{E}(t)+V_{AB}(\mathbf{R}). \quad (6)$$

The result was

$$M_{fi}^{(0)}(t,t') = -i\int_{t'}^{t} d\tau\langle\Phi_f^F(\tau)|V_F(\tau)|\Phi_i(\tau)\rangle, \quad (7)$$

which is the direct analog of the SFA for atoms.

Our aim is to generalize the theory presented in Ref. [24] so that it includes an additional interaction of the ionized electron with the atomic (ionic) centers. For this we will use an approach that is analogous to atomic HATI or atomic ATI with rescattering [5–7]. We will use the integral equation

$$U(t,\tau) = U_F(t,\tau)-i\int_{\tau}^{t} dt''U_F(t,t'')V_e^{AB}(\mathbf{r},\mathbf{R})U(t'',\tau), \quad (8)$$

where $U_F(t,\tau)$ is the evolution operator that corresponds to the Hamiltonian H_F. The potential $V_e^{AB}(\mathbf{r},\mathbf{R})$ defined in Eq. (5) describes the interaction of the ionized electron with the two molecular centers and is the analog of the atomic ATI

rescattering potential. Introducing Eq. (8) into Eq. (1) we obtain two terms. The first is given by Eq. (7) and describes the direct molecular ATI. It was considered in detail in Ref. [24]. The second term describes rescattering. Approximating again, in the spirit of the MSFA, $\Phi_f^* \to \Phi_f^{F*}$ and $U \to U_F$, it reduces to

$$M_{fi}^{(1)}(t,t') = -\int_{t'}^{t} d\tau \int_{\tau}^{t} dt'' \langle \Phi_f^F(t'')| \times V_e^{AB}(\mathbf{r},\mathbf{R}) U_F(t'',\tau) V_F(\tau) |\Phi_i(\tau)\rangle. \quad (9)$$

The evolution operator U_F can be expanded in terms of the wave vectors $|\Phi_j^F(t)\rangle$,

$$U_F(t,t') = \sum_j |\Phi_j^F(t)\rangle\langle\Phi_j^F(t')|. \quad (10)$$

Since the wave functions $\Phi_j^F(\mathbf{r},\mathbf{R},t)$ can be separated as

$$\Phi_j^F(\mathbf{r},\mathbf{R},t) = \phi_{e\mathbf{k}}(\mathbf{r},t)\phi_{AB\nu}(\mathbf{R},t), \quad (11)$$

where $\phi_{e\mathbf{k}}(\mathbf{r},t)$ is the electronic Volkov state in length gauge and $\phi_{AB\nu}(\mathbf{R},t)$ is the nuclear wave function (for their explicit forms see Ref. [24]), the summation over j includes the integration over the electron momenta $\mathbf{k}$ and the summation over the vibrational degree of freedom ν, i.e., $j \equiv \{\mathbf{k},\nu\}$. Denoting the final (drift) electron momentum by $\mathbf{p}_f$ and the initial and final vibrational degrees of freedom by ν_i and ν_f, respectively, for $t \to \infty$ and $t' \to -\infty$ we obtain $M_{fi}^{(1)}(\infty,-\infty) \equiv M_{fi}^{(1)}$, where

$$M_{fi}^{(1)} = -\sum_{\nu} \int d^3\mathbf{k} \int_{-\infty}^{\infty} dt \int_0^{\infty} d\tau \langle \Phi_{\mathbf{p}_f\nu_f}^F(t)|V_e^{AB}|\Phi_{\mathbf{k}\nu}^F(t)\rangle\langle\Phi_{\mathbf{k}\nu}^F(\tau') \times |V_F(\tau')|\Phi_{i\nu_i}^q(\tau')\rangle, \quad (12)$$

with $\tau' = t - \tau$. Here, in the initial state $\Phi_{i\nu_i}^q = \phi_{ei}^q \phi_{AB\nu_i}$, the initial electronic bound state can be field-free ($q=u$) or laser-dressed ($q=d$; see Sec. V in Ref. [24]).

We will fix the internuclear coordinate to the equilibrium position so that the electronic energy, the wave functions, and the matrix elements in Eq. (12) are calculated for $\mathbf{R} = \mathbf{R}_0$. The nuclear wave functions, $\phi_{AB\nu}(\mathbf{R},t) = \varphi_{AB\nu}(\mathbf{R})\exp(-iE_{AB\nu}t)$, in the case when the electron is ionized, are orthonormalized: $\langle \phi_{AB\nu_f}(t)|\phi_{AB\nu}(t)\rangle = \delta_{\nu\nu_f}$. On the other hand, the initial state is bound, while the final state is ionized, so that we have $\langle \phi_{AB\nu_f}(t)|\phi_{AB\nu_i}(t)\rangle = S_{\nu_f\nu_i}\exp[i(E_{AB\nu_f} - E_{AB\nu_i})t]$, where

$$S_{\nu_f\nu_i} = \int d^3\mathbf{R}\, \varphi_{AB\nu_f}^*(\mathbf{R})\varphi_{AB\nu_i}(\mathbf{R}) \quad (13)$$

is the overlap integral between the two vibrational states [24]. Therefore, the nuclear vibrational degree of freedom is contained only in the factor $S_{\nu_f\nu_i}$, similarly as it was obtained for the direct ATI amplitude in Ref. [24], and Eq. (12) reduces to

$$M_{fi}^{(1)} = -S_{\nu_f\nu_i} \int d^3\mathbf{k} \int_{-\infty}^{\infty} dt \int_0^{\infty} d\tau \langle \Phi_{e\mathbf{p}_f}^F(t)|V_e^{AB}|\Phi_{e\mathbf{k}}^F(t)\rangle\langle\Phi_{e\mathbf{k}}^F(\tau') \times |V_F(\tau')|\Phi_{ei}^q(\tau')\rangle \exp[i(E_{AB\nu_f} - E_{AB\nu_i})\tau'], \quad (14)$$

where all matrix elements are calculated at $\mathbf{R} = \mathbf{R}_0$. This expression is analogous to the rescattering matrix element for atomic HATI, so that the integral over $\mathbf{k}$, t, and τ can be calculated in the same way. Especially, these integrals can be treated using the saddle-point method, which will lead to a molecular version of quantum-orbit theory [5,7].

Let us now consider the continuum-continuum matrix element with the two-center rescattering potential $V_e^{AB}(\mathbf{r},\mathbf{R}) = V_e^A(\mathbf{r}_A) + V_e^B(\mathbf{r}_B)$. It can be shown that

$$\langle \mathbf{p}_f|V_e^J(\mathbf{r}_J)|\mathbf{k}\rangle = e^{i\mathbf{K}\cdot(\mathbf{r}-\mathbf{r}_J)} V_{e\mathbf{K}}^J \quad (J=A,B), \quad (15)$$

where $\mathbf{K} = \mathbf{k} - \mathbf{p}_f$ and $V_{e\mathbf{K}}^J$ is the Fourier transform of the rescattering potential at the atomic (ionic) center J

$$V_{e\mathbf{K}}^J = \int \frac{d^3\mathbf{r}}{(2\pi)^3} e^{i\mathbf{K}\cdot\mathbf{r}} V_e^J(\mathbf{r}) \quad (J=A,B). \quad (16)$$

We will model $V_e^J(\mathbf{r})$ by a static double Yukawa potential as in Refs. [26–28]. An example of the electron-molecule independent-particle model potential is presented in Ref. [29] for the N_2 molecule. For homonuclear diatomic molecules we have $M_A \approx M_B$ and $\lambda \approx 0$ so that

$$\langle \mathbf{p}_f|V_e^{AB}(\mathbf{r},\mathbf{R}_0)|\mathbf{k}\rangle = e^{-i\mathbf{K}\cdot\mathbf{R}_0/2} V_{e\mathbf{K}}^A + e^{i\mathbf{K}\cdot\mathbf{R}_0/2} V_{e\mathbf{K}}^B. \quad (17)$$

For a periodic laser field with period T, the result (14) can be further transformed similarly as it was done with the direct matrix element $M_{fi}^{(0)}$ in Ref. [24]. The S-matrix element $S_{fi} = \delta(\mathbf{P}_f^{\text{c.m.}} - \mathbf{P}_i^{\text{c.m.}}) M_{fi}(\infty,-\infty)$ is expressed through the T-matrix element for ionization with absorption of n photons from the laser field

$$S_{fi} = -2\pi i \delta(\mathbf{P}_f^{\text{c.m.}} - \mathbf{P}_i^{\text{c.m.}}) S_{\nu_f\nu_i} \sum_n \delta(\mathbf{p}_f^2/2 + \Delta E(\mathbf{R}_0) + U_p - n\omega) T_{fi}(n), \quad (18)$$

with $T_{fi}(n) = T_{fi}^{(0)}(n) + T_{fi}^{(1)}(n)$ and $\Delta E(\mathbf{R}_0) = E_{AB\nu_f} - E_{AB\nu_i} - E_{ei}(\mathbf{R}_0)$, while the corresponding ionization rate is $w_{fi}(n) = 2\pi p_f |T_{fi}(n)|^2$.

The molecular orbitals can be written as the linear combination of atomic orbitals (LCAO)

$$\sum_{J=A,B} \sum_a c_{Ja} \psi_a^{(0)}(\mathbf{r}_J), \quad (19)$$

where the sum over a denotes the sum over the atomic orbitals, while the sum over J denotes the sum over the centers A and B. These functions can be calculated using the standard software from quantum chemistry. For diatomic molecules we will use the self-consistent-field wave functions represented by linear combinations of Slater-type orbitals, which are obtained using the Hartree-Fock-Roothaan method [24]. For neutral homonuclear diatomic molecules, it is convenient to replace the summation index J by $s = \pm 1$, with the notation $\mathbf{r}_s = \mathbf{r} + s\mathbf{R}_0/2$, $\mathbf{r}_A = \mathbf{r}_{+1}$, $\mathbf{r}_B = \mathbf{r}_{-1}$. The matrix element (17) can be written as $\Sigma_s \exp(-is\mathbf{K}\cdot\mathbf{R}_0/2) V_{e\mathbf{K}}^s$, with $V_{e\mathbf{K}}^A \equiv V_{e\mathbf{K}}^{+1}$ and $V_{e\mathbf{K}}^B \equiv V_{e\mathbf{K}}^{-1}$.

Putting everything together, we obtain the T-matrix element $T_{fi}^{(j)}(n)$ $(j=0,1)$ as the Fourier transformation of the expression $\mathcal{F}_{fi}^{(j)}(t)\exp[i\mathcal{U}_f(t)]$,

$$T_{fi}^{(j)}(n) = \int_0^T \frac{dt}{T} \mathcal{F}_{fi}^{(j)}(t) e^{i\mathcal{U}_f(t)} e^{in\omega t}. \tag{20}$$

Here $\mathcal{U}_f(t) = \mathbf{p}_f \cdot \int^t d\tau \mathbf{A}(\tau) + \int^t d\tau \mathbf{A}^2(\tau)/2 - U_p t$, $\mathbf{A}(t) = -\int^t \mathbf{E}(\tau) d\tau$, and the explicit form of the function $\mathcal{F}_{fi}^{(j)}(t)$ depends upon which one of the various versions of the MSFA as introduced in Ref. [24] is used. We present here the final result for the dressed modified MSFA in length gauge for neutral homonuclear diatomic molecules [30]

$$\mathcal{F}_{fi}^{(0)d}(t) = \sum_s e^{is\mathbf{p}_f \cdot \mathbf{R}_0/2} \langle \mathbf{p}_f + \mathbf{A}(t) | \mathbf{r} \cdot \mathbf{E}(t) | \Psi_s^{(0)} \rangle, \tag{21}$$

$$\begin{aligned} \mathcal{F}_{fi}^{(1)d}(t) = & -ie^{-iS_{\mathbf{k}_{\mathrm{st}}}(t)} \int_0^\infty d\tau \left(\frac{2\pi}{i\tau} \right)^{3/2} e^{i[S_{\mathbf{k}_{\mathrm{st}}}(\tau') - \Delta E(\mathbf{R}_0)\tau]} \\ & \times \exp\left(-\frac{i}{2\tau} \frac{\partial^2}{\partial \mathbf{k}^2} \right) \sum_{s'} V_{e\mathbf{K}}^{s'} \sum_s e^{i(s\mathbf{k} - s'\mathbf{K}) \cdot \mathbf{R}_0/2} \\ & \times \langle \mathbf{k} + \mathbf{A}(\tau') | \mathbf{r} \cdot \mathbf{E}(\tau') | \Psi_s^{(0)} \rangle_{|\mathbf{k}=\mathbf{k}_{\mathrm{st}}}, \end{aligned} \tag{22}$$

where $|\Psi_s^{(0)}\rangle = \Sigma_a c_{sa} |\psi_a^{(0)}\rangle$, $\mathbf{k}_{\mathrm{st}} = \int_t^{\tau'} dt' \mathbf{A}(t')/\tau$, and $S_{\mathbf{k}}(t) = \int^t dt' [\mathbf{k} + \mathbf{A}(t')]^2/2$. The results for the undressed modified MSFA in length gauge can be obtained from Eq. (22) by the replacement

$$\exp(is\mathbf{q} \cdot \mathbf{R}_0/2) \rightarrow \exp\{is[\mathbf{q} + \mathbf{A}(\tau')] \cdot \mathbf{R}_0/2\}, \tag{23}$$

where $\mathbf{q} = \mathbf{p}_f$ for Eq. (21) and $\mathbf{q} = \mathbf{k}$ for Eq. (22).

B. Interference of the partial T-matrix contributions and the role of the molecular symmetry

In the previous subsection we have introduced our generalized MSFA. The ionization T-matrix element consists of six contributions

$$T = (T^+ + T^-) + (T^{++} + T^{--} + \tilde{T}^{+-} + \tilde{T}^{-+}) \tag{24}$$

[we have here dropped the subscripts and superscripts and the argument of $T_{fi}^{(j)}(n)$]. The first two terms T^+ and T^- come from the $s = \pm 1$ terms of the direct T-matrix element $T_{fi}^{(0)}(n)$ [see Eq. (21)]. The other four contributions T^{++}, T^{--}, $\tilde{T}^{+-}$, and $\tilde{T}^{-+}$ are the partial contributions to the rescattering T-matrix $T_{fi}^{(1)}(n)$, which is connected with the Fourier transform of Eq. (22). The two terms T^{++} and T^{--} refer to the situation where the electron is born at and rescatters off the same center, while in $\tilde{T}^{+-}$ and $\tilde{T}^{-+}$ these two events take place at different centers. Below, in Figs. 2–5, we will also employ the notation [31]

$$\begin{aligned} T^{+-} &\equiv T^+ + T^- + \tilde{T}^{+-}, \quad T^{-+} \equiv T^+ + T^- + \tilde{T}^{-+}, \\ T^{++--} &\equiv T^+ + T^- + T^{++} + T^{--}. \end{aligned} \tag{25}$$

These six contributions all lead into the same final state and, therefore, can interfere in a complicated manner. In addition, we have the sum over the atomic orbitals a. It should also be emphasized that each of the T-matrix contributions in the above equations consists of many contributions which correspond to different quantum paths (orbits) to the same final electron state [5,7]. Therefore, like in the atomic HATI, the "one-center" photoelectron spectra exhibit a reach interference structure apart from the two-center interference structures discussed below.

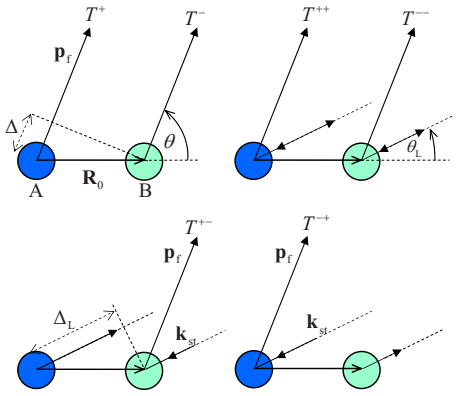

FIG. 1. (Color online) Schematic diagram of the six T-matrix contributions to the strong-field ionization of a molecule having two centers A and B. The electron with the final momentum $\mathbf{p}_f$ is emitted in the direction θ with respect to the relative nuclear coordinate $\mathbf{R}_0$. The laser field polarization vector and, in consequence, the intermediate rescattering electron momentum $\mathbf{k}_{\mathrm{st}}$ are in the direction θ_L. In the upper left panel the two direct ionization contributions (T^+ for the ionization at the center A and T^- for the center B) and the corresponding electron path difference Δ are presented. In the upper right panel the contributions T^{++} and T^{--}, where the electron rescatters at the same center at which it was born, are depicted. The two lower panels show the contributions of the processes where ionization and rescattering happen at different centers. The path difference of electrons in the lower left and lower right panels, before the rescattering, is $2\Delta_L$.

In spite of this seemingly complicated situation, it is possible to introduce a relatively simple physical picture of the ionization process. For this purpose, we will use Fig. 1, where we schematically present the aforementioned partial contributions to the ionization of the molecule ABe^- with internuclear separation R_0. The laser field polarization vector $\mathbf{e}_L$ is in the direction θ_L, i.e., $\theta_L = \angle(\mathbf{R}_0, \mathbf{e}_L)$, with respect to the molecular axis. The electron, having the final momentum $\mathbf{p}_f$, is emitted in the direction $\theta = \angle(\mathbf{R}_0, \mathbf{p}_f)$, also defined with respect to the molecular axis. The upper left panel of Fig. 1 presents the two direct ATI T-matrix contributions. It is clear that the phase difference between the two electron wave packets emitted from the center A (contribution T^+) and the center B (contribution T^-) is

$$p_f \Delta = p_f R_0 \cos\theta = \mathbf{p}_f \cdot \mathbf{R}_0 \equiv 2\alpha. \tag{26}$$

The interference of these contributions is destructive if $2\alpha = (2m+1)\pi$, which leads to the well-known condition for destructive interference of electrons with momentum $\mathbf{p}_f$ emitted from the two centers in the direction θ (see Refs. [16,20]):

$$E^{(+1)}_{\mathbf{p}_f,\min} = \frac{(2m+1)^2\pi^2}{2R_0^2\cos^2\theta}, \quad m = 0,1,2,\ldots . \tag{27}$$

The same formula, with modifications introduced by the molecular symmetry, can be derived using our formalism. In our notation, the connection between the coefficients c_{sa}, introduced in Eq. (19), depends on the symmetry of the considered molecule and is given by $c_{-1a}=s_{a\lambda}c_{1a}$, with

$$s_{a\lambda} = (-1)^{l_a-m_a}\begin{cases}(-1)^{m_\lambda} & \text{(for } g \text{ symmetry)},\\ (-1)^{m_\lambda+1} & \text{(for } u \text{ symmetry)}.\end{cases} \tag{28}$$

Here, m_λ is the projection of the orbital angular momentum on the internuclear axis. For example, for σ states it is $m_\lambda=0$, while for π states it is $m_\lambda=1$. The factor $(-1)^{l_a-m_a}$ comes from the inversion of the z coordinate of the second center. The summation over s in Eq. (21) gives the factor

$$F_{s_{a\lambda}}(\mathbf{p}_f\cdot\mathbf{R}_0) = e^{i\mathbf{p}_f\cdot\mathbf{R}_0/2} + s_{a\lambda}e^{-i\mathbf{p}_f\cdot\mathbf{R}_0/2}. \tag{29}$$

If, for all Slater-type atomic orbitals a that occur in the expansion of a given molecular orbital, the factor $(-1)^{l_a-m_a}$ has the same value (this is valid in the limit of large internuclear separation), then the factor (29) can be pulled out of the sum over a, i.e., the T-matrix element $T^{(0)}_{fi}$ is directly proportional to this factor. Since $F_{+1}(\mathbf{p}_f\cdot\mathbf{R}_0)=2\cos(\mathbf{p}_f\cdot\mathbf{R}_0/2)$ and $F_{-1}(\mathbf{p}_f\cdot\mathbf{R}_0)=2i\sin(\mathbf{p}_f\cdot\mathbf{R}_0/2)$, we will have a minimum in the electron spectrum for energies $E^{(s_{a\lambda})}_{\mathbf{p}_f,\min}$, where $E^{(+1)}_{\mathbf{p}_f,\min}$ is given by Eq. (27), and

$$E^{(-1)}_{\mathbf{p}_f,\min} = \frac{2(m+1)^2\pi^2}{R_0^2\cos^2\theta}, \quad m = 0,1,2,\ldots . \tag{30}$$

The conditions (27) and (30) will be further discussed in the next section, using numerical examples.

The two HATI contributions due to rescattering at the same center are presented in the upper right panel of Fig. 1. The electron ionized at one center goes in the direction θ_L and returns to the same center with the momentum $\mathbf{k}_{\rm st}$. Then the electron rescatters off this center and leaves the molecule going towards the detector in the direction θ with respect to the internuclear axis. The phase difference between the T^{++} and T^{--} contributions is the same as that for the T^{+} and T^{-} contributions and is given by Eq. (26), so that the minimum in the electron spectrum will again appear for the energies given by Eq. (27). This condition can also be obtained from our formalism: supposing that the contributions of $V^{+1}_{e\mathbf{K}}$ and $V^{-1}_{e\mathbf{K}}$ are approximately equal, the same factor (29) can be extracted from the partial T-matrix contribution $T^{++}+T^{--}$. This will again lead to the conditions (27) and (30). The condition (30) can also be understood in terms of destructive two-center electron emission in the following way. If we suppose that for $s_{a\lambda}=-1=\exp(i\pi)$ there is a phase difference π between the two centers (like the phase shift by π upon reflection from the more dense medium in optics), then the destructive interference condition has the form $2\alpha=(2m+1)\pi+\pi$, which corresponds to the condition that $T^{++}+T^{--}\propto\sin\alpha$ is minimal. This leads to condition (30).

To summarize, the T^{++--} contributions to the T matrix all exhibit the same manifestation of the two-center destructive interference, which is given by Eq. (27) or (30) depending on the value of $s_{a\lambda}$ characterizing the molecular symmetry. This is true provided all molecular orbitals have the same value of $s_{a\lambda}$.

Finally, the lower two panels of Fig. 1 depict the two HATI contributions due to rescattering at different centers. For the left (right) panel the electron is ionized from the center A (B), moves in the laser field, and returns to the center B (A), having the momentum $\mathbf{k}_{\rm st}$, where it rescatters and goes to the detector with the final momentum $\mathbf{p}_f$. From these two panels it is evident that the phase difference for these two contributions is

$$\begin{aligned}2k_{\rm st}\Delta_L - p_f\Delta &= 2k_{\rm st}R_0\cos\theta_L - p_fR_0\cos\theta\\ &= 2\mathbf{k}_{\rm st}\cdot\mathbf{R}_0 - \mathbf{p}_f\cdot\mathbf{R}_0 = 2\beta,\end{aligned} \tag{31}$$

$$\beta \equiv \mathbf{k}_{\rm st}\cdot\mathbf{R}_0 - \alpha. \tag{32}$$

The interference is destructive for $2\beta=(2m+1)\pi$. Our T-matrix formalism leads to the same destructive interference condition, i.e., we obtain that $\tilde{T}^{+-}+\tilde{T}^{-+}$ is proportional to $\cos\beta$ for $s_{a\lambda}=1$ symmetry. For $s_{a\lambda}=-1$, the additional phase π should be added to $(2m+1)\pi$, which is equivalent to the condition $\sin\beta=0$. And really, from Eq. (22) we obtain that $\tilde{T}^{+-}+\tilde{T}^{-+}\propto\sin\beta$ for $s_{a\lambda}=-1$.

We should add that the previous discussion was for the drift momenta and not for the velocities at the times of ionization or rescattering. The latter are time dependent, and it is not quite clear how to determine phase differences. In the dressed length gauge or in the velocity gauge, it is the drift momenta that appear in the Volkov solution, but this is not so in the undressed length gauge.

Let us now combine all rescattering T-matrix contributions

$$\begin{aligned}T^{(1)}_a &= (T^{++}+T^{--}+\tilde{T}^{+-}+\tilde{T}^{-+})_a\\ &\propto\begin{cases}\cos\alpha+\cos\beta = 2\cos\delta\cos\gamma & \text{for } s_{a\lambda}=+1,\\ \sin\alpha+\sin\beta = 2\sin\delta\cos\gamma & \text{for } s_{a\lambda}=-1,\end{cases}\end{aligned} \tag{33}$$

where

$$2\gamma \equiv \alpha-\beta = (\mathbf{p}_f-\mathbf{k}_{\rm st})\cdot\mathbf{R}_0, \quad 2\delta \equiv \mathbf{k}_{\rm st}\cdot\mathbf{R}_0. \tag{34}$$

The most important conclusion that follows from Eq. (33) is that the total rescattering contribution to the T matrix is proportional to $\cos\gamma$, so that $T^{(1)}_{fi}(n)\propto\cos\gamma=0$ for $2\gamma=(2m+1)\pi$, $m=0,1,2,\ldots$. Notice that this holds regardless of the values of $s_{a\lambda}$. That is, the molecular orbital may have components of different symmetry, and the two-center interference will be unaffected. Therefore, if we present the rescattering ionization rate in the $(E_{\mathbf{p}_f},\theta)$ plane, we will have local minima if the condition

$$R_0|p_f\cos\theta - k_{\rm st}\cos\theta_L| = (2m+1)\pi, \tag{35}$$

with m integer, is fulfilled. For $|k_{\rm st}\cos\theta_L| \ll |p_f\cos\theta|$ this reduces to the condition (27). For the laser and molecular parameters we are considering in the present paper only the lowest value $m=0$ contributes.

The result (33) with Eq. (34) is very instructive and one can learn a lot about the role of the molecular orientation and symmetry. If the molecular orientation is such that $\delta = \mathbf{k}_{st} \cdot \mathbf{R}_0/2$ is small, then the factor $\sin\delta$ and the contributions of the orbitals having $s_{a\lambda}=-1$ are also small. In this case, the contribution of the orbitals having $s_{a\lambda}=1$, for which $\cos\delta \approx 1$, is dominant. If, for example, in an experiment we find that for perpendicular molecular orientation the rescattering plateau is absent, we conclude that in the LCAO expansion of the molecular orbital of this molecule the contributions with $s_{a\lambda}=-1$ are dominant. This will be the case for the O_2 molecule (see Sec. III B). The same method can be used for other molecules. In addition, we have the factor $\cos\gamma$ both for $s_{a\lambda}=1$ and $s_{a\lambda}=-1$. The curve of the corresponding interference minima is characteristic of the molecule (which is described by the LCAO having both $s_{a\lambda}=1$ and $s_{a\lambda}=-1$) and can serve for the determination of, for example, the internuclear distance.

It can also be shown that $T_a^{(1)} \propto S_{l_a\lambda}(\mathbf{e}_L)$, where the real spherical harmonics $S_{l_a\lambda}(\mathbf{e}_L)$ are proportional to [32]

$$P_{l_a\lambda}(\cos\theta_L) \propto \sin^{\lambda}\theta_L \sum_{\nu=0}^{[(l_a-\lambda)/2]} \omega_{\nu}^{l_a\lambda} \cos^{l_a-\lambda-2\nu}\theta_L, \quad (36)$$

with $\lambda=|m_\lambda|=|m_a|$. This allows us to connect the rescattering contribution for a particular molecular orientation with the ath molecular constituent. We will use this to explain some of the results for the O_2 molecule.

In the case when the laser field polarization is perpendicular to the molecular axis ($\theta_L=90°$), the scalar product $\mathbf{k}_{st}\cdot\mathbf{R}_0$ in the phase of $\mathcal{F}_{fi}^{(1)d}(t)$, Eq. (22), vanishes, and we obtain

$$\sum_{s,s'} T^{ss'} \propto \sum_{s'} V_{e\mathbf{K}}^{s'} e^{is'\mathbf{p}_f\cdot\mathbf{R}_0/2} \sum_{s} c_{sa} \approx 2c_{1a}V_{e\mathbf{K}}^{1}\cos(\mathbf{p}_f\cdot\mathbf{R}_0/2)(1+s_{a\lambda}). \quad (37)$$

Therefore, for states having $s_{a\lambda}=-1$ the rescattering partial ionization rate vanishes, while for states having $s_{a\lambda}=1$ it is possible to observe minima, caused by the factor $\cos(\mathbf{p}_f\cdot\mathbf{R}_0/2)$, for energies $E_{\mathbf{p}_f\min}^{(+1)}$ given by Eq. (27).

III. NUMERICAL RESULTS

As examples we will consider the N_2 and O_2 molecules. For the N_2 molecule, the initial HOMO is $3\sigma_g$, so that the factor $(-1)^{m_\lambda}$ is equal +1 in Eq. (28). Twelve atomic orbitals with $m_a=0$ will be taken into account: $a=1s$, $1s'$, $2s$, $2s'$, $3s$, $2p$, $2p'$, $2p''$, $3d$, $3d'$, $3d''$, and $4f$. Therefore, for s states we have $s_{a\lambda}=1$, while for p states it is $s_{a\lambda}=-1$, etc. The HOMO of the O_2 molecule is $1\pi_g$, so that $(-1)^{m_\lambda}=-1$. We choose five atomic orbitals having $m_a=1$: $a=2p$, $2p'$, $2p''$, $3d$, and $4f$. For p and f states we have $s_{a\lambda}=-1$, while for d states it is $s_{a\lambda}=1$. The equilibrium internuclear distance of N_2 is $R_0=2.068$ a.u. and its ionization energy is $I_p=15.58$ eV. For O_2 we have $R_0=2.282$ a.u. and $I_p=12.03$ eV.

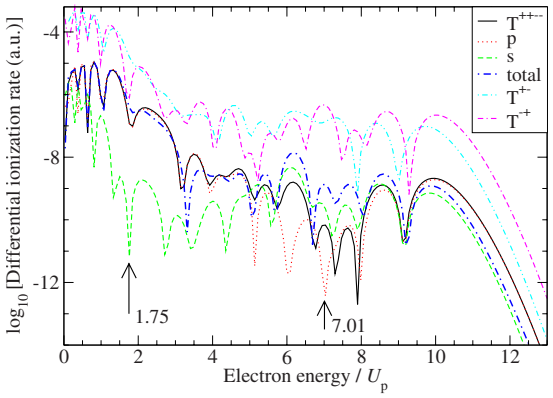

FIG. 2. (Color online) Logarithm of the differential ionization rate of N_2 as a function of the electron kinetic energy $E_{\mathbf{p}_f}$ in units of the ponderomotive energy U_p, for emission in the direction $\theta=0°$, for a linearly polarized laser field having the intensity 3×10^{14} W/cm^2 and the wavelength 800 nm. The angle between the molecular axis and the laser polarization axis is $\theta_L=0°$. The results are obtained using the improved dressed modified MSFA in length gauge (blue dot-dashed line denoted as "total"). Various partial contributions to the total rate are also exhibited, especially the contribution of only the s (green dashed line) and the p (red dotted line) components of the N_2 ground state wave function in the partial T-matrix element "T^{++--}." The remaining notation is explained in Eqs. (24) and (25). The curves "T^{+-}" and "T^{-+}," which correspond to the T^{+-} (cyan two-dots-dashed curve) and T^{-+} (magenta two-dash dotted curve) contributions to the T matrix, are shifted up by two orders of magnitude for better visual clarity.

A. Spectra of electrons emitted in the polarization direction: Analysis of the interference of partial T-matrix contributions

We will now present numerical results for HATI by a linearly polarized laser field with wavelength 800 nm for two values of the laser intensity $I_1=3\times10^{14}$ W/cm^2 (Fig. 2 for N_2 and Fig. 4 for O_2) and $I_2=4\times10^{14}$ W/cm^2 (Fig. 3 for N_2 and Fig. 5 for O_2). We consider electrons that are emitted in the polarization direction, so that $\theta=\theta_L$. According to the atomic $10U_p$-cutoff law [4,5,33], for these angles we expect to have high-energy electrons. For N_2 and O_2, we choose $\theta_L=0°$ and $\theta_L=45°$, respectively. In accordance with the cor-

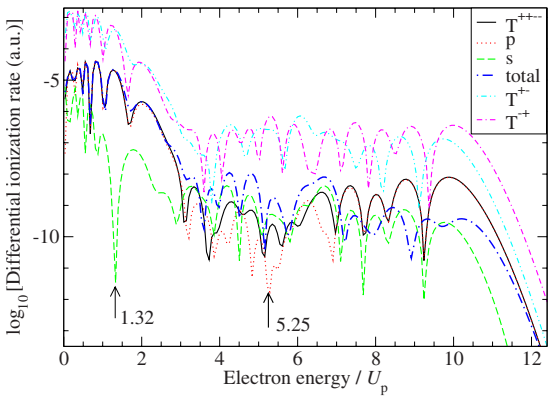

FIG. 3. (Color online) Same as in Fig. 2 but for the laser intensity 4×10^{14} W/cm^2.

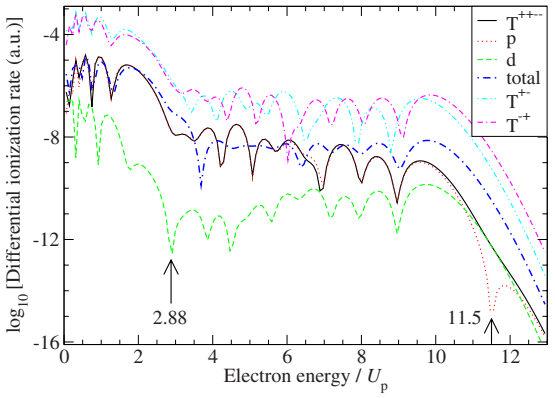

FIG. 4. (Color online) Same as in Fig. 2 but O_2, $\theta=\theta_L=45°$, and for p and d states.

responding ground-state wave functions and the results of Ref. [24], for these angles we expect the highest ionization rates.

For $\theta=0°$, Eqs. (27) and (30) for $I=I_1$ give $E^{(+1)}_{\mathbf{p}_f,\min}=1.75U_p$ and $E^{(-1)}_{\mathbf{p}_f,\min}=7.01U_p$, while for $I=I_2$ we have $E^{(+1)}_{\mathbf{p}_f,\min}=1.32U_p$ and $E^{(-1)}_{\mathbf{p}_f,\min}=5.25U_p$. Similarly, for O_2 and $\theta=45°$ we find $E^{(+1)}_{\mathbf{p}_f,\min}=2.88U_p$ and $E^{(-1)}_{\mathbf{p}_f,\min}=11.5U_p$ for $I=I_1$ and $E^{(+1)}_{\mathbf{p}_f,\min}=2.16U_p$ and $E^{(-1)}_{\mathbf{p}_f,\min}=8.63U_p$ for $I=I_2$. All these minimum energies are indicated by arrows in Figs. 2–5. In all figures the results that include all atomic orbitals are denoted by "total" (blue dot dashed line). The remaining notation is explained in the caption and in Eqs. (24) and (25).

It is evident in Figs. 2–5 that the "s," "p," and "d," results, which include only the contributions of the s, p, or d orbitals of the ground-state wave function in the partial T-matrix element T^{++--}, have minima for particular values of the electron energy, in accordance with the conditions (27) and (30). The minimum can be in the low-energy part of the spectrum, which is dominated by the direct electrons (see the "s" curve and the arrow at 1.32 in Fig. 3), in the plateau region ("p" curve and the arrow at 7.01 in Fig. 2), or even beyond the cutoff ("p" curve and the arrow at 11.5 in Fig. 4).

From Figs. 2–5 we also infer that without exception in the "total" results these minima are not present, either because the respective partial contribution is already insignificant in

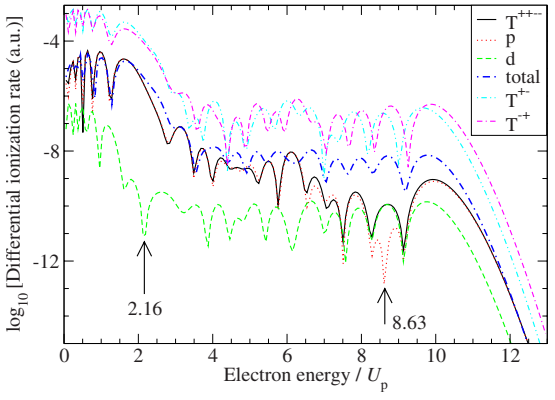

FIG. 5. (Color online) Same as in Fig. 3 but for O_2, $\theta=\theta_L=45°$, and for p and d states.

the term T^{++--} or, otherwise, because it is covered by the contribution of T^{+-} and T^{-+}. These terms come from electrons that are ionized at one molecular center and rescattered off the other. Such electrons normally absorb either more or less energy from the laser field than the electrons that rescatter off the same center at which they were ionized. The positions of the corresponding cutoffs can be different as one can see in Figs. 2–5: The cutoff of the T^{+-} contribution is lower than that of T^{-+}, while the cutoff of T^{++--} is in between the former two. The interference of all these contributions may give very complicated spectra, which depend on the laser parameters, electron emission angle, and the molecular orientation.

B. Angle and energy resolved molecular ATI spectra

1. The N_2 molecule

Figure 6 presents angle-resolved energy spectra for the N_2 molecule for four different orientations $\theta_L=0°$, 30°, 60°, and 90°. Similar results were already shown in Ref. [25]. Those were obtained using the dressed length-gauge modified MSFA—the same method we are using in the present paper. The spectra shown here were obtained using the undressed length-gauge modified MSFA. It can be shown that the considerations of Sec. II B remain the same in the case of the undressed length-gauge version of the modified MSFA if one replaces $\alpha\rightarrow\alpha+\mathbf{A}(\tau)\cdot\mathbf{R}_0$ and $\beta\rightarrow\beta+\mathbf{A}(\tau)\cdot\mathbf{R}_0$; cf. Eq. (23). This replacement does not affect the interference factor $\cos\gamma$, Eqs. (33) and (34). Therefore, using the undressed in place of the dressed length-gauge version of the modified MSFA does not affect the positions of the interference minima and maxima, although other details of the spectra may differ. This is confirmed by comparison of Fig. 6 of the current paper with the analogous figure in Ref. [25]. The conclusion is that undressed and dressed MSFA can equally well be used to explain the interference structures of molecular HATI. This holds for the cases that we investigated, for comparatively small internuclear separation. The two versions will more and more differ when this quantity increases.

Let us now analyze Fig. 6 in more detail. As expected, the cutoff is maximal for $\theta=\theta_L$. The spectra for $\theta_L=0°$ and $\theta_L=90°$ are symmetric with respect to the $\theta=\theta_L$ axis, while this symmetry is absent for $\theta_L=30°$ and $\theta_L=60°$. The most eye-catching feature of Fig. 6, which is most pronounced for $\theta_L=30°$ and 60°, is a broad one-to-two-orders-of-magnitude depression of the rescattering plateau in the angular region between $\theta=40°$ and 70°. This pattern is completely absent for an atom, see the corresponding spectrum for the companion atom of argon in Fig. 1(a) of Ref. [25]. The depression is the manifestation of destructive two-center interference [16]. The locus in the $(E_{\mathbf{p}_f},\theta)$ plane of its center is described by Eq. (35). A simple estimate of the quantity k_{st} in this equation may be obtained as follows. Recall from quantum-orbit theory that $k_{\mathrm{st}}=-\int_{t-\tau}^{t}d\tau' A(\tau')/\tau$ and that the shortest electron orbits correspond to ionization at the time $t-\tau$ near an extremum of the electric field and rescattering at the time t near the second-to-next zero crossing. For $A(t)=A_0\cos\omega t$, this means $\omega(t-\tau)\approx-\pi/2$ and $\omega t\approx\pi$, which gives $k_{\mathrm{st}}\approx$

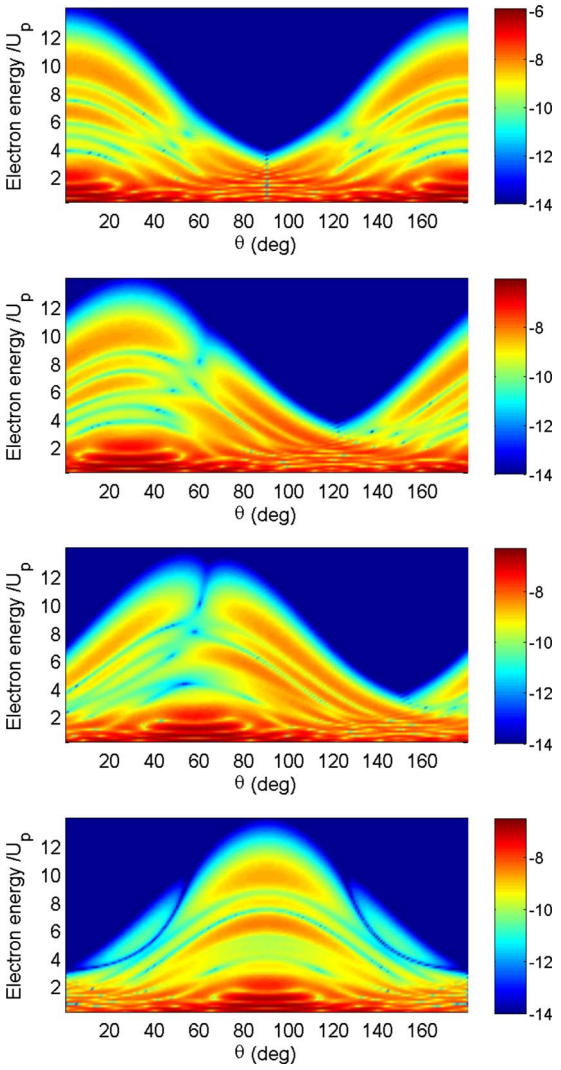

FIG. 6. (Color online) Logarithm of the differential ionization rate of N_2, coded in false colors in the $(E_{\mathbf{p}_f}, \theta)$ plane, for four different orientations of the molecular axis with respect to the polarization vector of the laser field, from the top to the bottom panel: $\theta_L = 0°$, 30°, 60°, and 90°. Intensity of the linearly polarized laser field is 1.68×10^{14} W/cm^2 and the wavelength is 800 nm. The results are obtained using the undressed length-gauge modified MSFA.

$-2A_0/(3\pi)$. Introducing this into Eq. (35), for $m=0$ we obtain

$$\left| p_f \cos\theta + \frac{2A_0}{3\pi} \cos\theta_L \right| = \frac{\pi}{R_0}. \tag{38}$$

This equation provides a good fit of the positions of the interference minima in the $(E_{\mathbf{p}_f}, \theta)$ plane, especially for $\theta_L = 90°$ where they are independent of k_{st}.

To confirm that the depression of the plateau is due to destructive two-center interference, we shall separately inspect the various contributions T^{++--}, $\tilde{T}^{+-}$, and $\tilde{T}^{-+}$. In Fig. 7 we present the electron energy spectrum for N_2 for $\theta_L = 60°$ at constant angle of emission $\theta = \theta_L = 60°$, which is near the center of the depression. Only the contribution of the atomic

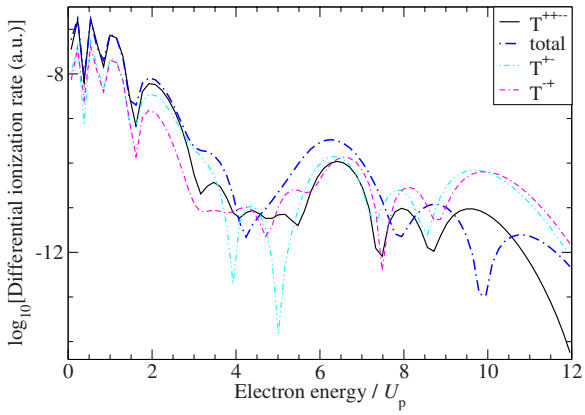

FIG. 7. (Color online) Logarithm of the differential ionization rates of N_2 as functions of the electron kinetic energy $E_{\mathbf{p}_f}$ in units of the ponderomotive energy U_p, for emission in the direction $\theta = 60°$, for $\theta_L = 60°$. The laser parameters are as in Fig. 6. The spectra are obtained using the dressed length-gauge modified MSFA and only the atomic *s* orbitals, which are dominant in the high-energy part of the spectrum of N_2. The total rate is denoted by total (blue dot-dashed line). The partial contributions T^{++--} (black solid line), T^{+-} (cyan two-dots-dashed curve), and T^{-+} (magenta two-dash dotted curve) are also presented.

s orbitals is taken into account since, for the laser parameters chosen, it is dominant in the high-energy part of the spectrum. From Fig. 7 we see that for $E_{\mathbf{p}_f} \approx 10U_p$ the T^{+-} and the T^{-+} contributions to the ionization rate are of comparable magnitude, while the T^{++--} contribution is lower than the former two by about one order. However, the coherent sum of all these contributions is lower by almost three orders of magnitude than the individual T^{+-} and T^{-+} contributions and still lower by two orders than T^{++--}. We have checked that for angles around $\theta = 60°$ these partial contributions each individually do not change very much and do not show any minima. The conclusion is that, first, there is very strong destructive interference between T^{+-} and T^{-+}. In addition, there is very strong destructive interference between $T^{+-} + T^{-+}$ on the one hand and T^{++--} on the other, which then leads to the very strongly depressed total result. The precise position of these interference minima depends on the laser parameters via the quantity k_{st} in Eq. (35), i.e., Eq. (38). For example, for $I = 0.9 \times 10^{14}$ W/cm^2 the minima are near $\theta = 50°$, while for $I = 3 \times 10^{14}$ W/cm^2 they are at $\theta \approx 70°$.

Clearly, the dominant feature of the angle-resolved electron-energy spectrum is the massive depression of the rescattering plateau, which is caused by destructive two-center interference. However, as we just realized, interference between the same-center contribution T^{++--} and the cross-over contribution $T^{+-} + T^{-+}$ is also important. Indeed, for near-parallel or near-perpendicular orientation, Fig. 6 shows that two-center destructive interference does not affect the spectra around emission angles $\theta \approx \theta_L$ [34]. However, interference between same-center and cross-over contributions does. For another example of the latter type of interference, consider Figs. 2 and 3: In Fig. 3, for $E_{\mathbf{p}}$ near $10U_P$, the total rate is below the same-center rate T^{++--} by one order of magnitude. Apparently, this must be due to destructive interference with the different-center contribution $T^{+-} + T^{-+}$. In

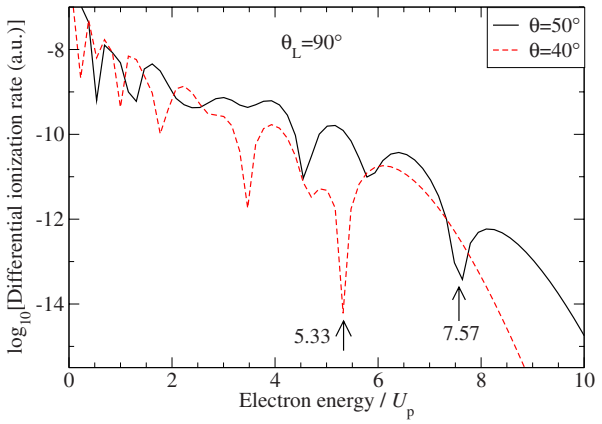

FIG. 8. (Color online) Logarithm of the differential ionization rates of N_2 as functions of $E_{\mathbf{p}_f}/U_p$, for emission in the direction $\theta=40°$ (red dashed curve) and $\theta=50°$ (black solid curve). The results are obtained using the dressed length-gauge modified MSFA. The laser parameters are as in Fig. 6 and $\theta_L=90°$.

contrast, in Fig. 2 at the lower intensity of 3×10^{14} W/cm^2, the total rate is only very slightly below the same-center rate. In consequence, the yield of rescattered electrons in the upper part of the plateau is below the yield of direct electrons by 4 to 5 orders of magnitude for the higher intensity of Fig. 3 and only by 3 to 4 orders for the lower intensity of Fig. 2.

Next, we focus on the case of perpendicular molecular orientation ($\theta_L=90°$). As we have shown in the last paragraph of Sec. II B [see Eq. (37)], in this special case, the atomic orbitals having $s_{a\lambda}=-1$ do not contribute to the rescattering ionization rate, while the contribution of the orbitals having $s_{a\lambda}=1$ (s and d orbitals for our N_2 example) is proportional to $\cos(\mathbf{p}_f\cdot\mathbf{R}_0/2)$. Therefore, according to Eq. (27) (for $m=0$), the ionization rate will have minima for energies and angles satisfying the condition

$$E_{\mathbf{p}_f}\cos^2\theta=\frac{\pi^2}{2R_0^2}. \tag{39}$$

Two examples of these minima are shown in Fig. 8. For $\theta=40°$ the minimum appears at $E_{\mathbf{p}_f}=5.33U_p$, while for $\theta=50°$ it is at $E_{\mathbf{p}_f}=7.57U_p$. The figure shows that these minima are very sharply defined, unlike the broad depressions of the rescattering plateau discussed above. This is particularly evident from the lowest panel of Fig. 6. Therefore, Eq. (39) is very well suited for the determination of the equilibrium internuclear distance from the measured electron spectra. In Ref. [25], we have shown that this curve survives focal averaging. However, there is a price to be paid for the sharpness of the interference curve. Namely, it is located near, if not slightly outside, the classical boundary, where the electron count is comparatively low.

For $\theta_L\neq90°$ the term proportional to $k_{\mathrm{st}}\cos\theta_L$ in Eq. (35) becomes important. Since k_{st}^2 is proportional to the laser intensity, focal averaging blurs the interference minima picture. This was clearly shown in the upper panel of Fig. 2 in Ref. [25], where the focal-averaged spectra for $\theta_L=0°$ were presented.

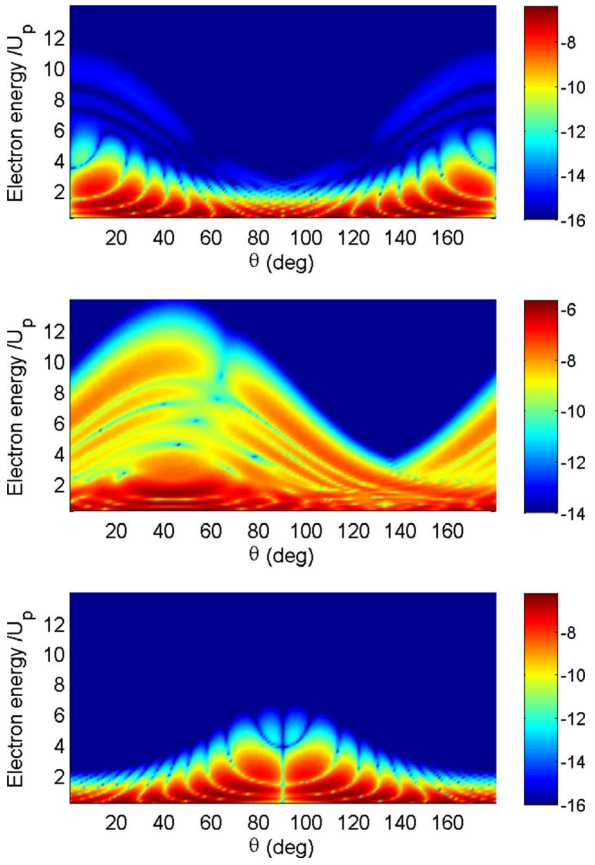

FIG. 9. (Color online) Logarithm of the differential ionization rate of O_2, coded in false colors in the $(E_{\mathbf{p}_f},\theta)$ plane, obtained using the undressed length-gauge modified MSFA, for three different orientations of the molecular axis with respect to the polarization vector of the laser field $\theta_L=0.01°$ (upper), 45° (middle), and 90° (bottom panel). The presentation and the laser parameters are as in Fig. 6.

2. The O_2 molecule

We now turn our attention to the energy and angle-resolved spectra of the O_2 molecule. In Fig. 9, we present an example of the angle and energy resolved spectra of O_2, obtained using the undressed modified MSFA. These results are analogous to those obtained by the dressed modified MSFA, presented in Fig. 3 in Ref. [25], and the results are qualitatively the same. Due to the π symmetry of the O_2 ground-state wave function, the corresponding spectra are quite different from those of N_2. For molecular alignment along the nodal line $\theta_L=0°$, the high-energy plateau is absent for O_2. (In the upper panel of Fig. 9, the value $\theta_L=0.01°$ was used, which is the reason of the presence of a very weak plateau). The differential ionization rate is maximal for $\theta_L=45°$, in which case the plateau extends to energies above $10U_p$ (for $\theta=45°$) and its height is comparable to that of N_2. For $\theta_L=90°$ the high-energy plateau is again absent. This is in accordance with Eq. (37) and the fact that for O_2 the partial contribution of p atomic orbitals, for which $s_{a\lambda}=-1$, is dominant. Also, it can be shown analytically [see Eq. (36)] that the contribution of the d orbital is proportional to $\cos\theta_L$, which is zero for perpendicular alignment. In Fig. 3 of Ref.

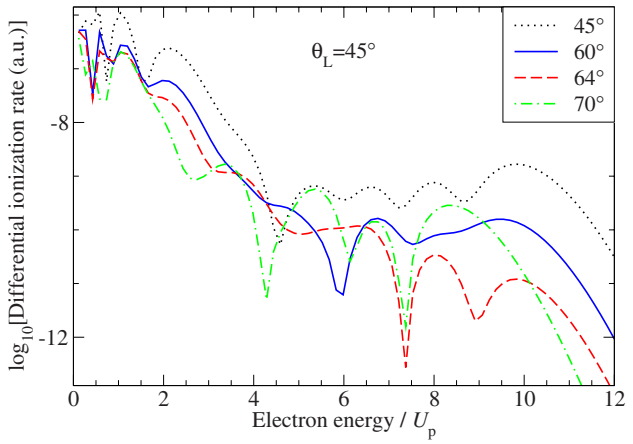

FIG. 10. (Color online) Logarithm of the differential ionization rates of O_2 as functions of $E_{\mathbf{p}_f}/U_p$, for emission in the direction $\theta=45°$ (black dotted curve), 60° (blue solid curve), 64° (red dashed curve), and 70° (green dot-dashed curve). The results are obtained using the dressed length-gauge modified MSFA. The laser parameters are as in Fig. 6 and $\theta_L=45°$.

[25] the calculations have been done for $\theta_L=1°$ and $\theta_L=89°$ in order to show how the plateaus start to appear for alignments which are not exactly parallel or perpendicular (of course, these plateaus are below the detection threshold).

For $\theta_L=45°$, we observe similar to N_2 a deep depression in the rescattering plateau, which again approximately follows the curve given by Eq. (38). In Fig. 10, we investigate the suppressed plateau more closely by plotting several spectra at constant angle of emission. The interference minima predicted by Eq. (38) are clearly visible: for $\theta=60°$, 64°, and 70° they appear at $E_{\mathbf{p}_f}/U_p=5.9$, 7.4, and 7.4, respectively. But the important point is that as for N_2 these minima mark the center of a very broad valley. For $\theta=45°$ the plateau is still well developed. At $\theta=60°$ it is already suppressed by one order of magnitude; at 64° the upper part of the plateau is two orders of magnitude below the average height for $\theta=45°$, and at 70° it has not fully recovered yet. Also, for $\theta=70°$ an additional minimum appears for $E_{\mathbf{p}_f}=4.3U_p$.

Comparing Figs. 2 and 3 for N_2 with Figs. 4 and 5 for O_2, we notice that for O_2 the total rate is larger than each partial rate for either intensity. Correspondingly, for O_2 the plateau has a relatively higher yield than for N_2. We also observe that fewer and less deep "canyons" cut into the plateau for O_2 than for N_2 [35]. This is just an observation based on the spectra calculated. The partial rates T^{++--}, T^{+-}, etc. fluctuate on the same scale for both N_2 and for O_2, but for some reason the total rate is much smoother for O_2 than for N_2.

IV. CONCLUSIONS

We have generalized the strong-field approximation theory of molecular ATI, developed in Ref. [24], so that it includes electron rescattering off the atomic (ionic) centers of a diatomic molecule to first order. In the fixed-nuclei approximation the intermediate vibrational states do not influence the ionization process. For equilibrium internuclear distances the length of the high-energy rescattering plateau is close to that of atomic HATI ($10U_p$). However, the plateau structure of the molecular spectra is different from that of atomic spectra and strongly depends on the molecular symmetry and the orientation of the molecule. This is reflected in the appearance of minima for particular values of the electron energy and emission angle. Some of these interference minima are connected with the symmetry properties of the particular atomic orbitals that form the molecular ground state. They can be masked by the contributions of atomic orbitals having different parity. The rescattering matrix element consists of four contributions: two come from the electron rescattering off its parent (ionic) center and the other two from rescattering off the other (atomic) center. The interference of all these contributions can also mask and destroy the aforementioned minima. It is difficult to find the conditions under which all of these contributions interfere destructively. By analyzing these spectra for different values of the angle θ_L, which determines the molecular orientation with respect to the laser polarization axis, and for different values of the electron emission angle θ, we were able to draw some conclusions about the structure of the electron spectra for different molecular symmetries. Furthermore, we have derived analytical conditions for the appearance of minima in these spectra and we have illustrated this using the examples of the N_2 ($3\sigma_g$ HOMO) and the O_2 ($1\pi_g$) molecules. The condition (35) and its dominant-quantum-orbits version (38) predict the position of the two-center destructive interference fairly well. For high electron energy, it occurs around emission angles of $\theta\approx 60°$ (with respect to the internuclear axis) regardless of the molecular orientation. When $\theta\approx\theta_L$, this interference all but eliminates the high-energy part of the rescattering plateau (see Fig. 6). For the N_2 molecule, conditions (35) and (38) can also be employed for the determination of the equilibrium internuclear distance. For the O_2 molecule both for exactly parallel and for exactly perpendicular orientation the rescattering plateau is absent, while for $\theta_L=45°$ the electron spectra are similar to those of the N_2 molecule.

In the present paper we have used the fixed nuclei approximation, i.e., we have supposed that the internuclear distance is fixed during the HATI process. If the internuclear distance changes on the time scale of the rescattering process, i.e., $R=R(\tau)$, where τ is the electron travel time, then the dynamic two-center interference is possible. This has been recently observed in high-order harmonic generation [36], and it has been shown that the interference occurs at lower harmonic order than would be the case if the nuclei were static. We expect that the effect of the dynamic interference will be similar for HATI, i.e., the interference minima will shift to lower energies.

We have shown that there are different aspects of the molecular symmetry which are connected with the rescattering matrix element. For example, the interchange of g and u symmetry changes the interference type and for π symmetry the ionization rate is proportional to $\sin^2\theta_L$. Our theory is general and is not limited to the cases of N_2 and O_2. Therefore, it can serve as a sensitive tool for molecular characterization. This approach can easily be generalized to multicenter molecules, using the simple physical picture of the ionization process that was introduced in Sec. II B (compare Fig. 1).

ACKNOWLEDGMENTS

We gratefully acknowledge support by the Volkswagen-Stiftung, by the Ministry of Education and Science, Canton Sarajevo, and by the Federal Ministry of Education and Science, Bosnia and Herzegovina.

[1] A. Becker and F. H. M. Faisal, J. Phys. B **38**, R1 (2005).
[2] P. B. Corkum, Phys. Rev. Lett. **71**, 1994 (1993).
[3] K. J. Schafer, B. Yang, L. F. DiMauro, and K. C. Kulander, Phys. Rev. Lett. **70**, 1599 (1993).
[4] G. G. Paulus, W. Nicklich, H. Xu, P. Lambropoulos, and H. Walther, Phys. Rev. Lett. **72**, 2851 (1994).
[5] W. Becker, F. Grasbon, R. Kopold, D. B. Milošević, G. G. Paulus, and H. Walther, Adv. At., Mol., Opt. Phys. **48**, 35 (2002).
[6] D. B. Milošević and F. Ehlotzky, Adv. At., Mol., Opt. Phys. **49**, 373 (2003).
[7] D. B. Milošević, G. G. Paulus, D. Bauer, and W. Becker, J. Phys. B **39**, R203 (2006).
[8] A. Scrinzi, M. Yu. Ivanov, R. Kienberger, and D. M. Villeneuve, J. Phys. B **39**, R1 (2006).
[9] T. Zuo, A. D. Bandrauk, and P. B. Corkum, Chem. Phys. Lett. **259**, 313 (1996).
[10] H. Niikura, F. Légaré, R. Hasbani, A. D. Bandrauk, M. Yu. Ivanov, D. M. Villeneuve, and P. B. Corkum, Nature (London) **417**, 917 (2002).
[11] S. N. Yurchenko, S. Patchkovskii, I. V. Litvinyuk, P. B. Corkum, and G. L. Yudin, Phys. Rev. Lett. **93**, 223003 (2004).
[12] M. Spanner, O. Smirnova, P. B. Corkum, and M. Yu. Ivanov, J. Phys. B **37**, L243 (2004).
[13] T. Morishita, A. T. Le, Z. Chen, and C. D. Lin, Phys. Rev. Lett. **100**, 013903 (2008).
[14] J. Itatani, J. Levesque, D. Zeidler, H. Niikura, H. Pépin, J. C. Kieffer, P. B. Corkum, and D. M. Villeneuve, Nature (London) **432**, 867 (2004).
[15] V.-H. Le, A.-T. Le, R.-H. Xie, and C. D. Lin, Phys. Rev. A **76**, 013414 (2007).
[16] M. Lein, J. Phys. B **40**, R135 (2007).
[17] A. D. Bandrauk, S. Chelkowski, and I. Kawata, Phys. Rev. A **67**, 013407 (2003).
[18] M. Lein, J. P. Marangos, and P. L. Knight, Phys. Rev. A **66**, 051404(R) (2002).
[19] C. C. Chirilă and M. Lein, Phys. Rev. A **74**, 051401(R) (2006).
[20] H. Hetzheim, C. Figueira de Morisson Faria, and W. Becker, Phys. Rev. A **76**, 023418 (2007).
[21] S. X. Hu and L. A. Collins, Phys. Rev. A **73**, 023405 (2006).
[22] F. Grasbon, G. G. Paulus, S. L. Chin, H. Walther, J. Muth-Böhm, A. Becker, and F. H. M. Faisal, Phys. Rev. A **63**, 041402(R) (2001).
[23] M. Okunishi, K. Shimada, G. Prümper, D. Mathur, and K. Ueda, J. Chem. Phys. **127**, 064310 (2007).
[24] D. B. Milošević, Phys. Rev. A **74**, 063404 (2006).
[25] M. Busuladžić, A. Gazibegović-Busuladžić, D. B. Milošević, and W. Becker, Phys. Rev. Lett. **100**, 203003 (2008).
[26] A. Čerkić and D. B. Milošević, Phys. Rev. A **70**, 053402 (2004); Laser Phys. **15**, 268 (2005).
[27] D. B. Milošević, A. Gazibegović-Busuladžić, and W. Becker, Phys. Rev. A **68**, 050702(R) (2003); A. Gazibegović-Busuladžić, D. B. Milošević, and W. Becker, *ibid.* **70**, 053403 (2004).
[28] E. Hasović, M. Busuladžić, A. Gazibegović-Busuladžić, D. B. Milošević, and W. Becker, Laser Phys. **17**, 376 (2007).
[29] T. Sawada, P. S. Ganas, and A. E. S. Green, Phys. Rev. A **9**, 1130 (1974).
[30] We favor the dressed modified MSFA in length gauge in accordance with the results of W. Becker, J. Chen, S. G. Chen, and D. B. Milošević, Phys. Rev. A **76**, 033403 (2007). Numerical comparison of different versions of the MSFA for the direct ATI was presented in Ref. [24]. We have checked that the numerical results for all versions of the rescattering molecular ATI qualitatively agree.
[31] Actually, when in the figures we label some partial T-matrix contribution with, say, T^{++--} we do not plot this amplitude but rather its square $|T^{++--}|^2$. This should not lead to confusion.
[32] A. C. Wahl, P. E. Cade, and C. C. J. Roothaan, J. Chem. Phys. **41**, 2578 (1964).
[33] M. Busuladžić, A. Gazibegović-Busuladžić, and D. B. Milošević, Laser Phys. **16**, 289 (2006).
[34] For $\theta_L=90°$, the two-center interference perpendicular to the molecular axis ($\theta=90°$) is always constructive for N_2 by symmetry, so that there cannot be any interference minima. In contrast, for $\theta_L=0°$ destructive interference does occur for $\theta=0°$. However, for the parameters of Fig. 6, the $m=0$ destructive interference is at very low energy and the next ($m=1$) destructive interference is already at an energy far outside the figure.
[35] The origin of these "canyons," which are comparatively steep and narrow, is essentially the same as in atoms and has little to do with the presence of two centers. They are caused by destructive interference of the molecular analogs of "the long" and "the short" orbit as well as "longer" orbits. A quantitative understanding would require developing the molecular extension of quantum-orbit theory.
[36] S. Baker, J. S. Robinson, M. Lein, C. C. Chirilă, R. Torres, H. C. Bandulet, D. Comtois, J. C. Kieffer, D. M. Villeneuve, J. W. G. Tisch, and J. P. Marangos, Phys. Rev. Lett. **101**, 053901 (2008).